CrossMark

RESEARCH PAPER

Quantum mechanical investigation of optoelectronic properties of gold nanoparticle attached titanium dioxide nanorods for device applications

Dhyey Raval · Brijesh Tripathi ⬤ · Abhijit Ray

Abstract This article reports gold nanoparticle (Au-NP) induced absorption enhancement in hydrothermally synthesized titanium dioxide nanorods (TiO_2-NRs) with a possibility of the deposition of hybrid nanostructures on the transparent substrates. The localized surface plasmon resonance (LSPR) and hot electron transfer behaviour of Au-NPs attached to the TiO_2-NRs has been correlated to their photocatalytic response. The photocurrent enhancement observed in amperometric studies has been explained on the basis of excess electron density in the conduction band of TiO_2 due to hot electron transfer from the attached Au-NPs (size in the range of 3 to 44 nm). The quantum mechanical calculation of the electron transmission probability from the resonant Au-NP to the conduction band of TiO_2-NR has been presented with respect to the wavelength of the incident spectrum. Further, the role of Au-NP size dependent electron work function has been correlated to the electron transmission probability. This study provides a quantum mechanical explanation to the better response of Au-NPs/TiO_2-NRs system for photo-catalytic device applications.

Keywords Titanium dioxide nanorods · Gold nanoparticles · Photocatalysis · Plasmon · Hot electron · Quantum effects

D. Raval · A. Ray
Department of Solar Energy, School of Technology, Pandit Deendayal Petroleum University, Gandhinagar 382007, India

B. Tripathi (✉)
Department of Science, School of Technology, Pandit Deendayal Petroleum University, Gandhinagar 382007, India
e-mail: brijesh.tspv@gmail.com

Introduction

Titanium dioxide (TiO_2)-based heterostructures make use of a narrow band gap semiconductor and noble metal nanostructures (Chen and Mao 2007; Liu et al. 2010; Wang et al. 2010) to spread the light-response range to the visible region and improve the charge separation and transfer properties of micro-optical devices for photo-electro-catalysis (Lee et al. 2016). These novel heterostructures combine different electronic properties of the constituent materials and promote photo-catalytic efficiency as compared to the single-phase TiO_2 photo-catalyst (Baker and Kamat 2009; Tada et al. 2006; Zhang et al. 2008). The TiO_2 nanorods show better charge transport properties compared to the TiO_2 NP-based mesoporous layer (Kim et al. 2013a). Noble metal nanoparticles (NPs) on the surface of TiO_2 nanorods (NRs) can improve the photo-catalytic properties in mainly two ways: (A) the deposited noble metal nanoparticles behaves as an electron trap and enhances electron-hole separation to improve the quantum yield (Lidia et al. 2007; Paramasivam

et al. 2008; Zhang et al. 2008), (B) surface plasmon resonance (SPR) effect, which occurs due to the collective and coherent electronic oscillations on the noble metal nanoparticles through visible light irradiation. These effects can enhance the localized electric field in the vicinity of the metal nanoparticles, which helps in the interaction of the localized electric fields with a neighbouring semiconductor and allows the facile formation of electron-hole (e^--h^+) pairs in the near-surface region of the semiconductor/metal nanoparticle interface (Awazu et al. 2008; Ingram and Linic 2011; Thimsen et al. 2011; Xu et al. 2010). Recently, the localized surface plasmon resonance (LSPR) effects of Au-NPs and other metal nanostructures have been used to boost the photo-electrochemical properties and attracted wide research attention due to their possible application in micro-optical (Feng et al. 2016; Sun et al. 2015; Zhang et al. 2016) and photo-catalytic devices (Erwin et al. 2016; Huang et al. 2016; Lee et al. 2016). Multi-core flat fibre structure-based surface plasmon resonance sensor has been demonstrated by Rifat et al. (2016), which indicated a possibility of integrated SPR sensor as a lab-on-a-chip for the real-time diagnostic purpose. Awazu and Linic have used the plasmon enhanced photo-catalytic mechanism by isolating Ag NPs using SiO_2 and poly (vinylpyrrolidone) (PVP) as shells, respectively (Awazu et al. 2008; Ingram and Linic 2011). Liu et al. (2011) proposed an effective plasmon coupled photo-catalyst for splitting H_2O molecules under visible light by integrating Au NPs with doped TiO_2 nanotubes. The literature indicates that the plasmon resonance wavelength and intensity strongly depends on the size and shape of NPs, inter-particle spacing, and dielectric property of the surrounding medium (El-Sayed 2001; Feldstein et al. 1997; Feng et al. 2011; Lin et al. 2005; Rycenga et al. 2011).

In recent research, noble metal NPs, such as Pt (Xu et al. 2007a; Zhou et al. 2003), Pd (Liang et al. 2009; Qi et al. 2014), Ag (Fu et al. 2015; Liang et al. 2011) and Au (Chen et al. 2012; Cherevko et al. 2012), exhibited good catalytic activity for electro-oxidation and became the most common catalysts (Jin et al. 2016). Meanwhile, many efforts have been made to improve the activity and stability of noble metal NPs, such as development of NPs with specific surface structure (Cui et al. 2011; Qi et al. 2014; Xu

et al. 2007b) and with different alloying contents (Dutta et al. 2011; Oliveira et al. 2011; Wang et al. 2014; Zhu et al. 2012). In addition, photo-electro-catalysis has attracted much attention because of the outstanding LSPR properties, which improve the catalytic activity of noble metal NPs (Hutter and Fendler 2004). The recombination of photo-generated hot electrons and holes reduces the effect of LSPR (Wang et al. 2012; Wu et al. 2011). This recombination can be reduced by combining noble metal NPs with semiconductors to transfer the excited hot electrons into the conduction band (CB) of the adjacent semiconductor, which is defined as plasmon-induced charge separation (Bian et al. 2013; Tian and Tatsuma 2005) and has been proved to be beneficial for electro-oxidation (Murdoch et al. 2011; Tian and Tatsuma 2005; Xu et al. 2011). Since light illumination enhances the electro-oxidation activity, a periodic nanostructure consisting of noble metallic catalysts to enhance the incident light harvesting may be a promising method (Kim et al. 2013b). The vertically aligned titania nanorods (TiO_2-NRs) can be more beneficial for plasmon induced photo-catalysis due to one-dimensional facile charge transfer possibility (Raval et al. 2016). However, there are few attempts towards explaining these aspects of the metal nano-structures to enhance the plasmon resonance energy to improve the photo-catalytic activities of semiconductor materials (Long et al. 2017; Yen et al. 2017).

This article reports the hydrothermal synthesis of TiO_2-NRs with and without gold nanoparticles on their surface. These samples have been characterized by X-ray diffraction (XRD), field emission scanning electron microscopy (FE-SEM) and amperometric measurements. It is observed that the Au-NPs significantly improve the photo-catalytic response of TiO_2-NRs, which has been explained through a quantum mechanical approach. Theoretical calculations have been done to explore the extinction efficiency of the Au-NPs on TiO_2-NRs.

Theoretical description

Band diagram and electron transfer

The charge carriers gain energy through LSPR under visible light irradiation at Au/TiO_2 interface and get transferred to the conduction band of

TiO$_2$ from the gold NPs as shown in Fig. 1. It can be understood from Fig. 1 that the Au-NPs mainly act as a sensitizer, which absorb incident photons and generate the energetic hot electrons due to the process of the LSPR excitation. The highly energetic hot electrons get injected into the CB of the adjacent TiO$_2$-NRs (Zhang et al. 2012). Resonant Au-NPs exhibit optically induced oscillating electrostatic potential under illumination with respect to the wavelength of incident light (van de Groep et al. 2016). The excess electron density in the conduction band of TiO$_2$-NR plays a role in the photo-response of the TiO$_2$-NR/Au-NP system (Reineck et al. 2016). The transmission probability of generated hot electrons in Au-NPs through the potential barrier of TiO$_2$-NR can be calculated using Eqs. (1–6) (Ghatak 2010) under following assumptions: (1) Junction existing in between Au-NP and TiO$_2$-NR material acts as a potential barrier, (2) Fermi energy levels of Au-NP and TiO$_2$-NR remain aligned during photon interaction with potential barrier.

$$\frac{\partial^2 \Psi_1(x)}{\partial x^2} + k_1^2 \Psi_1(x) = 0, x$$
$$< 0 \ Designated \ as \ region \ 1 \ (Au\text{-}NP) \qquad (1)$$

$$\frac{\partial^2 \Psi_2(x)}{\partial x^2} + k_2^2 \Psi_2(x) = 0, \ x > 0 \qquad (2)$$

Designated as region 2 (TiO$_2$-NR)

where,

$$k_1^2 = \frac{2mE_0}{\hbar^2}, k_2^2 = \frac{2m(E_0 - V)}{\hbar^2}, m = 9.1 \times 10^{-31} kg, \hbar$$
$$= \frac{h}{2\pi} = 1.054 \times 10^{-34} Js.$$

The solutions of Eqs. (1) and (2) represent the wave functions of electron on the Au-NP and TiO$_2$-NR side as given by:

$$\Psi_1 = A e^{-jk_1 x} + B e^{jk_1 x} \qquad (3)$$

$$\Psi_2 = C e^{-jk_2 x} \qquad (4)$$

Under following boundary conditions:

1) The wave function is continuous at the interface, i.e. $\Psi_1(0) = \Psi_2(0)$, which implies that A + B = C from Eq. (3).
2) The first derivate of the wave function is continuous i.e. $\frac{\partial}{\partial x}\Psi_1(0) = \frac{\partial}{\partial x}\Psi_2(0)$, which implies that A−B = $\frac{k_2}{k_1}$ C from Eq. (4).

From these expressions transmission (T) and reflection (R) probability of electrons from Au-NPs through the TiO$_2$-NRs potential barrier can be calculated using following equations:

$$T = \left|\frac{B}{A}\right|^2 = \left|\frac{k_1 - k_2}{k_1 + k_2}\right|^2 \qquad (5)$$

$$R = \left|\frac{C}{A}\right| \frac{k_2}{k_1} = \frac{4k_1 k_2}{|k_1 + k_2|^2} \qquad (6)$$

Extinction efficiency calculations

The diameter of the particle must be well below the wavelength of light. The scattering and absorption cross section are given by (Bohren and Huffman 2007):

$$C_{scat} = \frac{1}{6\pi}\left(\frac{2\pi}{\lambda}\right)^4 |\alpha|^2 \qquad (7)$$

$$C_{abs} = \frac{2\pi}{\lambda} Im[\alpha] \qquad (8)$$

where, $\alpha = 3V\left[\frac{\varepsilon_p/\varepsilon_m - 1}{\varepsilon_p/\varepsilon_m + 2}\right]$ denotes polarizability of the particle. Here, V denotes particle volume (a function of particle radius), ε_p denotes the dielectric function of the particle, and ε_m denotes the dielectric function of the embedding medium. This expression shows that the scattering cross section depends on the NP size, and as a result, more fraction of light is scattered towards the medium with a higher refractive index. This is clearly observed by enhanced absorption as shown in Fig. 2, the Au-NPs attached TiO$_2$-NR layer is higher as compared to bare TiO$_2$-NRs. However, when the size of Au-NP increases beyond threshold limit, the phase retardation effect dominates (Westcott et al. 2002) and higher order multipole excitation modes (quadrupole, octupole) result in the decreased efficiency of the scattering
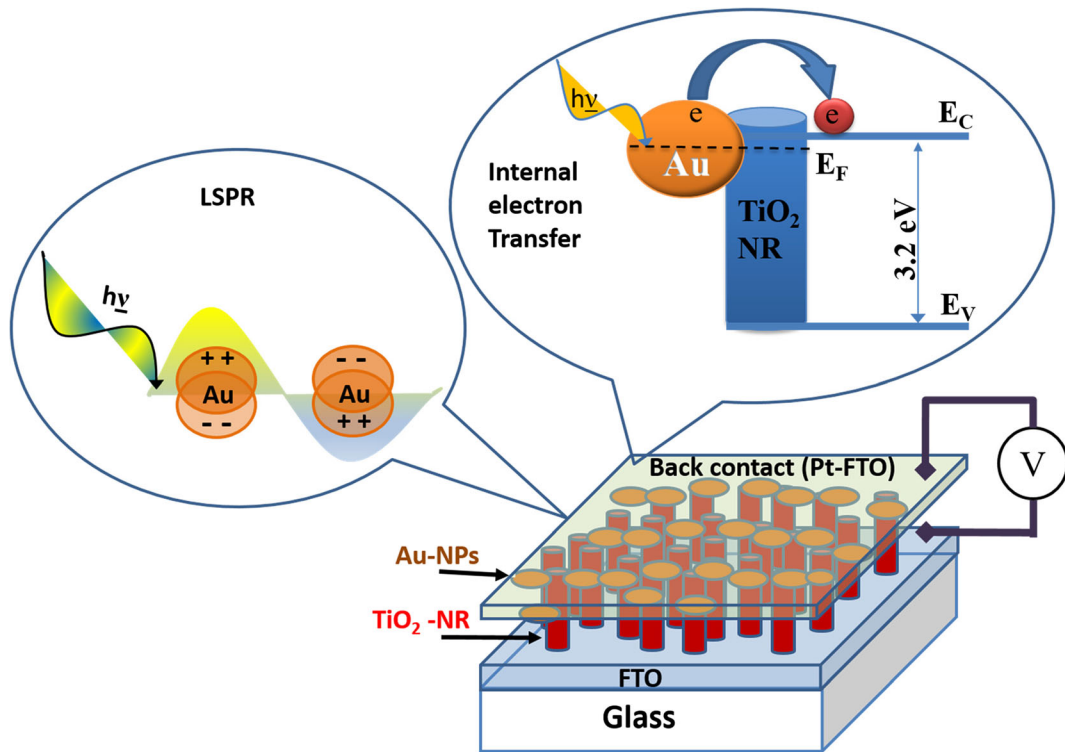
Fig. 1 Schematic diagram to represent physical processes in Au-NP/TiO$_2$-NR-based device

process(Bing et al. 2010). The size of Au-NP could be optimized by controlling the thickness of the Au thin film during the deposition process and followed by temperature. The extinction efficiency ($Q_{ext} = C_{scat}/S + C_{abs}/S$, S being an effective area of scattering particle) of Au-NPs is calculated using Mie theory(Tripathi et al. 2013) and shown in Fig. 3. The plasmon extinction evolves with the increase in the size of Au-NPs, which is in accordance with the existing literature (Huang and El-

Fig. 2 Optical characterization of TiO$_2$-NR and Au-NP/TiO$_2$-NR. Inset **a** Diffuse reflectance of TiO$_2$-NR and Au-NP/TiO$_2$-NR. Inset **b** Transmittance of Au-NP on glass substrate
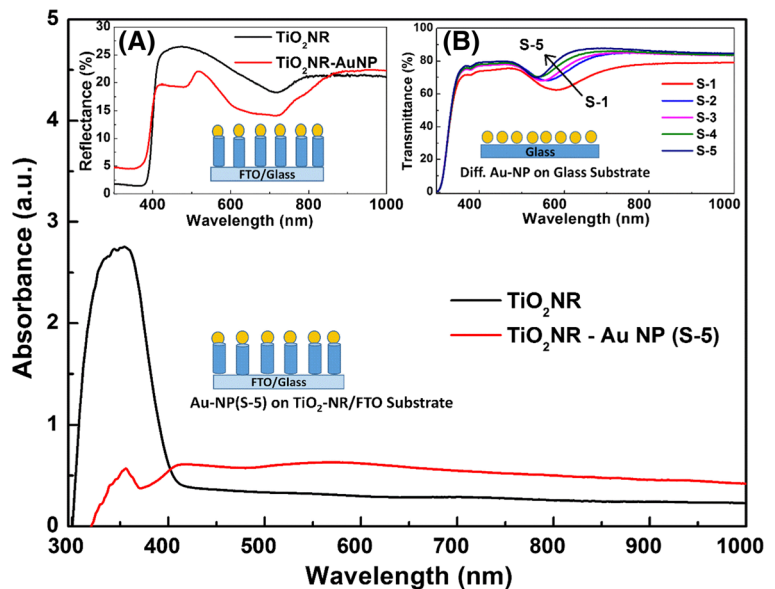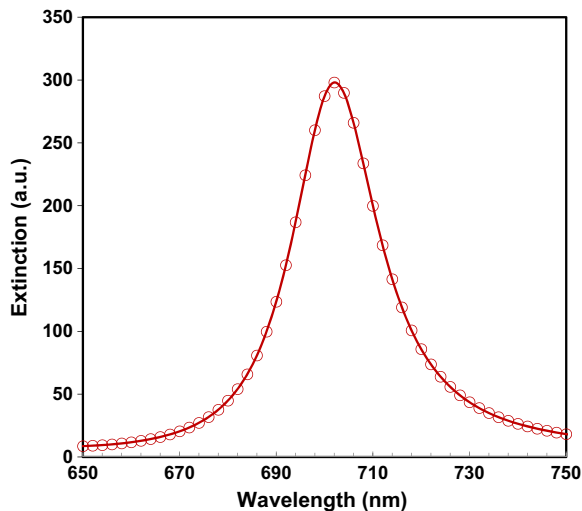
Fig. 3 Extinction (Q_{ext}) of Au nanoparticles on TiO_2-NR

Sayed 2010; Jain et al. 2006). The increase in particle size leads to an increased contribution from Mie scattering.

The incident light is lost through the sample surface by radiative and non-radaitive mechanisms. The scattering efficiency, Q_{sca} quantifies radiative loss and absorption efficiency, Q_{abs} quantifies non-radiative loss. These losses are included in the extinction efficiency, Q_{ext}, which effectively includes Q_{sca} and Q_{abs}, and can be calculated for spheres much smaller than the wavelength using the well-known Mie theory (Bohren and Huffman 2007).

Experimental section

Synthesis of materials

Fluorine-doped tin oxide (FTO) coated glass substrate (7 Ω/square, Sigma-Aldrich) substrates were used to grow TiO_2-NRs. A stainless steel autoclave of 50 mL capacity with Teflon lining has been used for the hydrothermal synthesis of TiO_2 nanorods. In a typical synthesis step, 15 mL of 37% hydrochloric acid was added in the 15 mL of deionized water and sonicated for 5 min. Subsequently, 0.4 mL of titanium (IV) isopropoxide ($Ti(OCH(CH_3)_2)_4$, 97%, Sigma-Aldrich) was added and further sonication did for 5 min. FTO glass substrates (1.5 cm × 1.5 cm) were placed inside the Teflon (melting point: 326.8 °C) liner with the active layer facing the wall for TiO_2-NR deposition. The prepared

precursor solution was then poured into an autoclave containing the substrates. The reaction time duration was set to 2 h and the process temperature was 230 °C. After completing the hydrothermal process, the autoclave was left to naturally cool down to room temperature. The substrates were taken out from the autoclave, rinsed thoroughly, and annealed at 300 °C in air prior to use. For depositing Au, a gold target (99.9%) (2-in. diameter, 3 mm thickness) has been used in RF/DC pulsed magnetron (10 kHz, duty cycle: 50%) sputtering system (Millman, Pune). Argon gas was injected with the constant flux of 50 sccm while maintaining working pressure at 8×10^{-2} mbar during the entire coating process. The sputtering of Au is done at an applied voltage of 350 V. The process current is measured to be ∼40 mA for 1-min time duration and temperature was close to 450 °C. All the samples were annealed (1 h), in a vacuum, after film deposition. The samples cooled down freely in vacuum before their removal to room conditions (Raval et al. 2016).

Morphological, structural and optical characterization

The morphological, structural and optical properties of TiO_2-NRs were examined by field emission scanning electron microscopy (FE-SEM, ULTRA55, Zeiss), energy dispersive spectrometer (EDS, Model: X-Max, Make: OXFORD), atomic force microscopy (Nanosurf Easycan 2), X-ray diffraction (XRD, X'Pert Pro, PANalytical) in the 2θ range of 20–80° and diffuse reflectance spectroscopy (UV 2600, Shimadzu) respectively.

Electrochemical characterization

For the electrochemical measurements, a working electrode (TiO_2-NR with and without Au-NPs in either case) and a platinized FTO as a counter electrode were placed in fixed positions in the testing cell with 0.5 M KOH electrolyte solution. A calibrated LED light source with an intensity of 20 mW/cm^2 with an optical chopper was placed between the light source and the photo-electrode for the photocurrent measurement. The photocurrent density was determined with the stable output signals from the test cell connected to the potentiostat (CHI-660D) without any applied bias (See Supplementary Information for more details).

Results and discussion

Structural analysis

Figure 4 shows the X-ray diffraction (XRD) spectrum of the hydrothermally grown TiO_2-NRs on FTO glass substrates, where the diffraction peaks are identified as the rutile phase according to JCPDS 21-1276 card. Generally, rutile TiO_2 powder containing randomly oriented crystals show a higher (110) diffraction intensity as can be seen in the JCPDS reference of Fig. 4, which is similar to the reported data for the rod-shaped rutile TiO_2 nanoparticles (Park et al. 1999). However, in the present case Fig. 4 the (101) diffraction intensity is highest, whereas the (110) peak intensity is comparatively low. This deviation in the intensity for the rutile TiO_2-NRs has been confirmed by other researchers also (Kim et al. 2013a). An intense (101) peak along with the enhanced (002) peak for the TiO_2-NR layer shows that the rutile crystal grows with (101) plane parallel to the FTO glass substrate and the nanorods are aligned with the (002) direction (Kim et al. 2013a; Nayak et al. 2012;
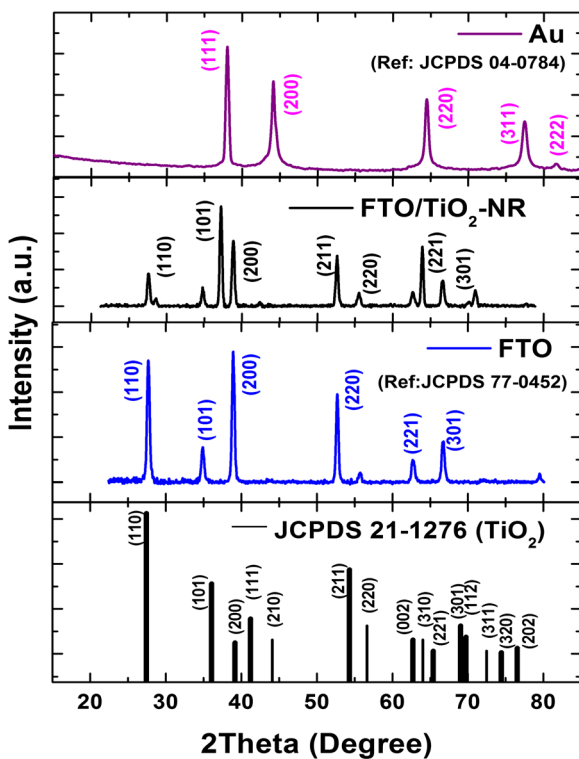

Fig. 4 XRD pattern for TiO_2-NR on FTO and Au-NPs. JCPDS 77-0452 corresponds to crystallographic planes of FTO. JCPDS 21-1276 corresponds to crystallographic planes of TiO_2. JCPDS 04-0784 corresponds to crystallographic planes of Au

Zhang and Liu 1998). The XRD pattern for the gold nanostructures is shown in Fig. 4, which illustrates prominent peaks corresponding to the (111), (200), (220) planes of face centered cubic (FCC) crystal structure of Au. This result is in agreement with the existing data for gold nanoparticles (JCPDS card number-04-0784) (Zhao et al. 2014). The peak intensity from (111) plane is higher than the other peaks, which confirms the presence of NPs. The preferred orientation in XRD pattern leads to spherical morphology as confirmed from FE-SEM image (Fig. 6) e.

Morphological and elemental analysis

The morphology of the bare TiO_2-NRs and Au-NPs incorporated with TiO_2-NRs has been investigated by FE-SEM and corresponding images are shown in Fig. 5a. The TiO_2 layer prepared by hydrothermal method with subsequent heat treatment at 230 °C for 2 h, exhibit nanometre size NRs morphology. FE-SEM images of Au-NP incorporated TiO_2-NRs are shown in Fig. 5b. The TiO_2-NR layer has porous morphology, wherein the pores are several hundred nanometres wide as observed in the FE-SEM images top-view of Fig. 5a. The diameter of TiO_2-NR is in the range of 80 ± 5 nm Fig. 5a. Figure 5b shows Au-NPs deposited over TiO_2-NR layer. The inset of Fig. 5b shows the size distribution of the Au-NPs. Au-NPs of 15 nm size with a variation of ± 10 nm are observed. The cross-sectional image of combined TiO_2-NRs and Au-NPs layer deposited on FTO coated glass substrate is shown in Fig. 5c. The thickness of FTO layer is estimated to be 293 ± 10 nm, thickness of TiO_2 seed layer is 700 ± 10 nm and thickness of TiO_2-NRs layer is 2241 ± 10 nm from Fig. 5c. The EDS of the Au-NPs/TiO_2-NRs confirms presence of Au, Ti, O as shown in Fig. S1 in Supplementary Information. The detailed profile elemental analysis was done cross-sectional through EDS for Au-NPs/TiO_2-NRs as shown in Fig. 5d. In Fig. 5d, the blue curve shows approximate concentration (in %) of oxygen with respect to the cross sectional thickness, green curve shows approximate concentration (%) of titanium and red curve shows approximate concentration (%) of gold. Region I shows a higher percentage of Au than TiO_2 and confirms that the Au-NPs are on the top of each NR as it is also seen in top view in Fig. 5b. In Fig. 5d, region II shows a higher percentage of TiO_2 than Au over that thickness range. Au percentage decreases in region II to zero, which confirms that there is no direct contact
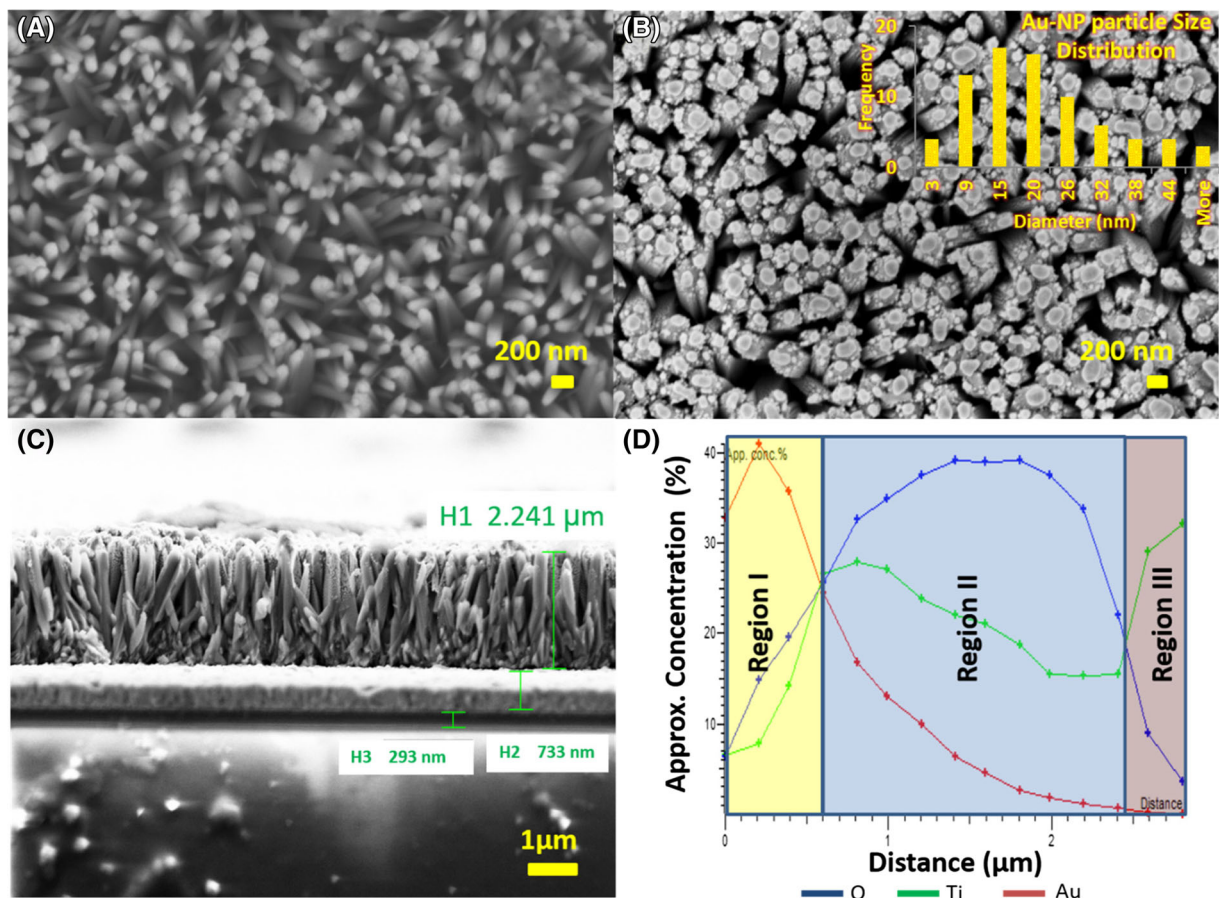
Fig. 5 FESEM and EDS characterization. **a** Top view of the TiO$_2$-NRs. **b** Au-NPs on TiO2-NRs with size distribution. **c** Cross-sectional view of the TiO$_2$-NRs. **d** Elemental cross-sectional profile distribution of Ti, Au, O in Au/TiO$_2$ sample

between FTO layer and Au-NPs. Region III shows titanium rich seed layer. Figure 5d clearly distinguishes different layer concentration over different thickness range. The size distribution of Au-NPs is shown in Fig. 6 (FE-SEM image of Au-NP coated TiO$_2$-NRs). The morphological characterization has been carried out by atomic force microscopy (AFM). The AFM has been performed in the tapping mode using a Nanosurf Easyscan2 system. The AFM images have been recorded at different positions with a scan area of 500 × 500 nm^2. The Au NP/TiO$_2$ NR layer morphology is shown in Fig. 6a. Figure 6b shows height distribution of Au-NP decorated on hydrothermally grown TiO$_2$-NR on FTO substrate. The AFM micrograph displayed a uniform distribution of a granular TiO$_2$-NR structure which is consistent with a high-quality and pin-hole free, smooth and crack-free surface as reported by other researchers (Sciancalepore et al. 2008). The histogram of the layer represents the hills corresponding to its average height (nm) distribution. A topographical analysis of the film is also shown in Fig. 6c–d in a 3D view. The 3D view of TiO$_2$-NR and TiO$_2$ NR/Au-NP with a color scale bar shows vertically oriented TiO$_2$-NRs and Au-NPs.

Optical analysis

UV-vis analysis

In Fig. 2, the results of UV-Vis spectroscopic measurements are presented. The absorbance spectra are plotted with respect to the wavelength of incident radiation for a bare TiO$_2$-NR sample and it is compared with TiO$_2$-NR/Au-NP sample. It is seen clearly that TiO$_2$-NR/Au-NP sample has much larger absorption in the visible range (> 400 nm) than the TiO$_2$-NR sample. There are mainly four types of energy-transfer mechanisms in a plasmonic photocatalytic system (Linic et al. 2011) (1) transfer of a
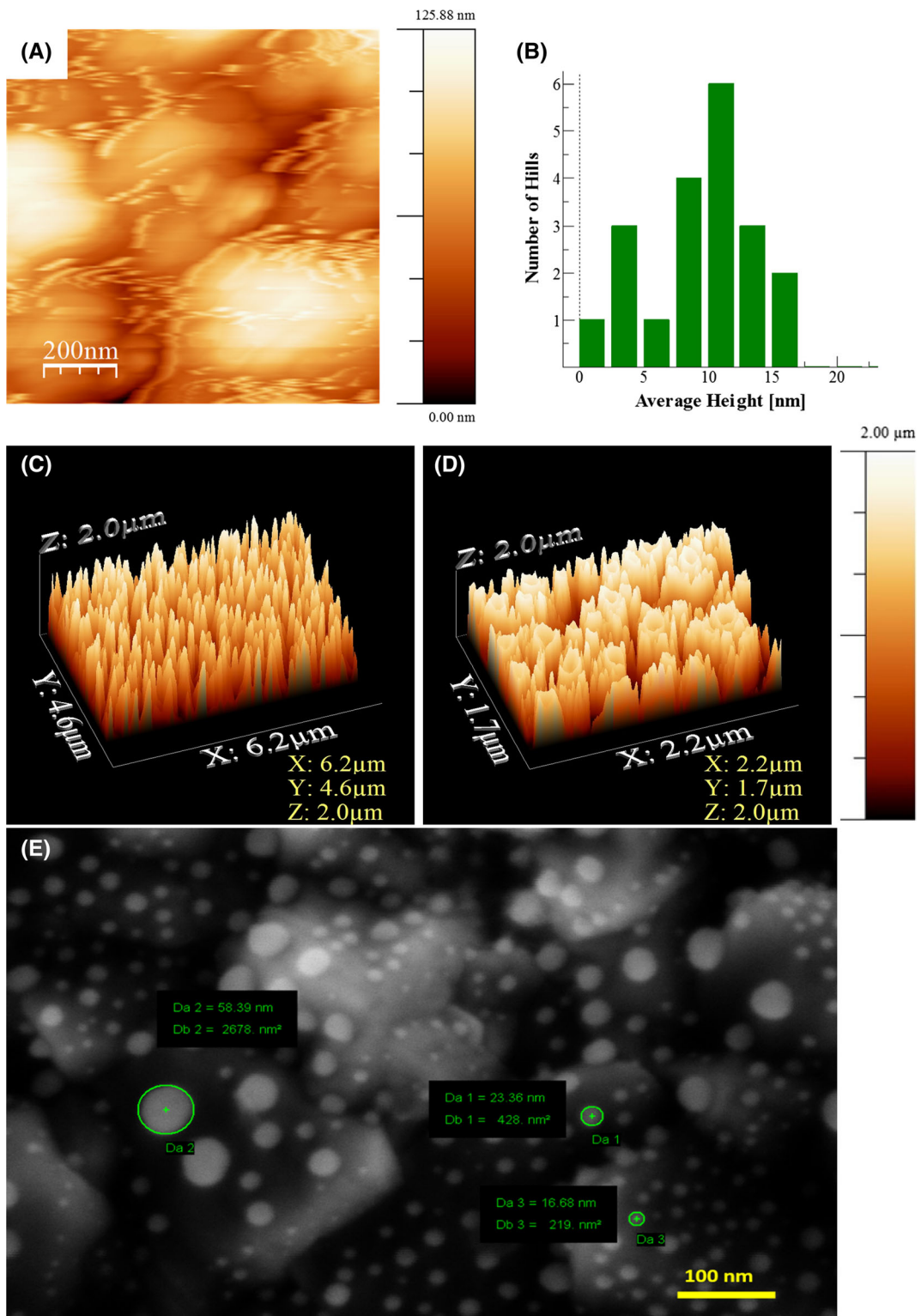
Fig. 6 Atomic force microscopy of **a** TiO$_2$-NR/Au-NP morphology. **b** Height distribution of TiO$_2$-NR/Au-NP. A topographical 3D view of **c** TiO$_2$-NR and **d** TiO$_2$-NR/Au-NP. **e** FE-SEM image of Au-NPs/TiO$_2$-NRs showing the distribution of Au-NPs

hot electron, (2) plasmon induced heating, (3) electromagnetic enhancement through near-field, and (4) resonance in photon scattering. The energy associated with plasmonic heating is significantly lower than the bandgap of TiO$_2$-NR thus it is not a leading mechanism to increase the carrier density in the CB of TiO$_2$-NRs (Liu et al. 2011). The resonant photon-scattering mechanism may not be prevailing mechanism in case of the Au-NP/TiO$_2$-NRs, as it normally occurs for large plasmonic NPs (larger than ~ 50 nm in diameter) (Burda et al. 2005; Evanoff and Chumanov 2005). Further, electromagnetic enhancement due to near-field is generally observed at wavelengths where the plasmon resonance and semiconductor absorption overlap so this is not a dominant mechanism of the charge transfer (Warren and Thimsen 2012). In the present case, the hot electron are generated by the absorption of incident radiation (hν > 0.9 eV), which is explained in next section. Hot electron transfer mechanism is responsible for the absorption enhancement and is a major contributor to improve the charge concentration in the conduction band of TiO$_2$ which enhances the performance of the Au/TiO$_2$-NRs-based devices under visible light illumination. The broadening of the absorption peak in the visible and near infra-red range is mainly due to the non-uniformity of Au nanoparticle size (Bian et al. 2013). The decrease in the absorbance of Au/TiO$_2$-NRs in ultra-violet region is due to lower exposed surface of the TiO$_2$-NRs as it is covered by Au-NPs. The reflection and transmission measurement of corresponding samples are shown in insert (A) & (B) of Fig. 2. The inset (A) of Fig. 2 shows the reduced reflection of incident radiation due to Au-NPs over TiO$_2$-NRs. The inset (B) of Fig. 2 shows the effect of size of nanoparticles (on glass) on the transmittance of incident radiation. The arrow shows direction of decrease in the size of Au-NPs.

Electrical analysis

Quantum mechanical explanation of the electron transfer from Au-NP to TiO$_2$-NRs

The potential step offered by the conduction band of TiO$_2$-NRs at the Au-NP/TiO$_2$-NR interface is shown in the Fig. 7a. The barrier height (V) is calculated from the difference of gold NP work function (ϕ, varies from 3.6
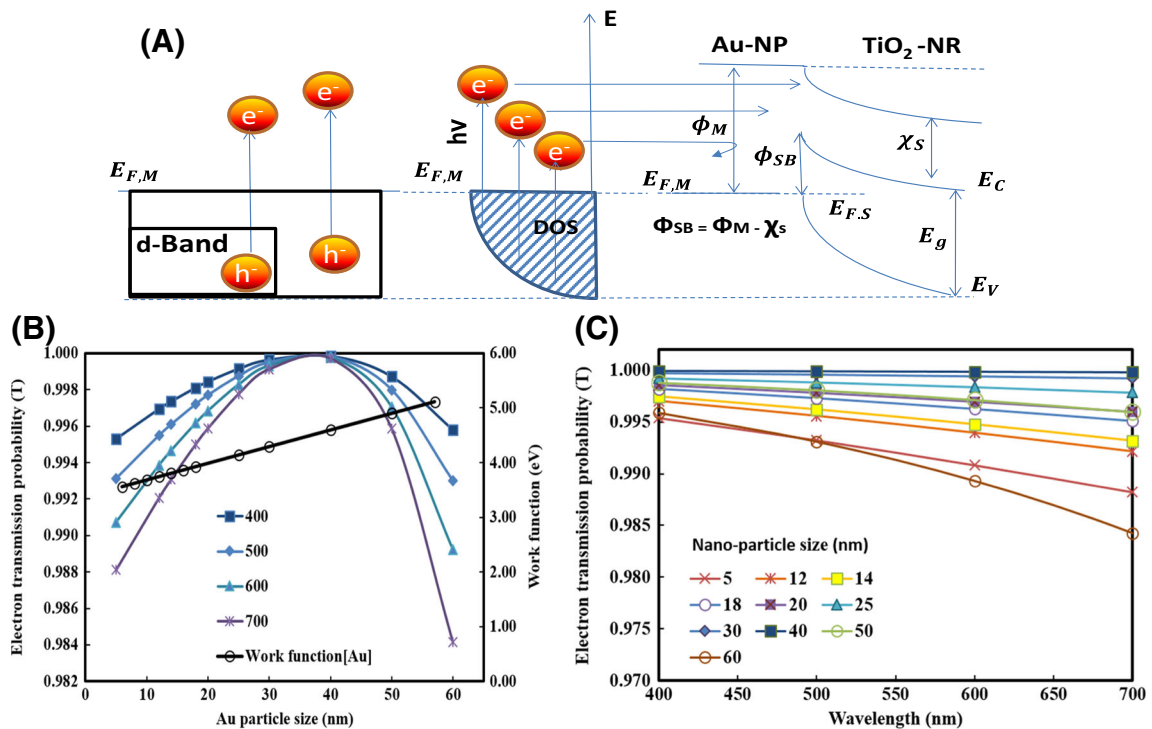

Fig. 7 a Excitation of electrons through the incident spectral photons with the mechanism of transfer from Au-NP to TiO$_2$-NR and corresponding Schrodinger wave equations representing the movement of the electrons. **b** Electron transmission probability with respect to Au-NP size and corresponding work function. **c** The electron transmission probability with respect to the wavelength of incident radiation assuming complete energy transfer from the corresponding photon to the electrons in Au-NP

to 5.1 eV (Zhang et al. 2015) and TiO_2 electron affinity (4.5 eV) (Sarkar et al. 2012). The plasmonic oscillations are responsible for an increase in the energy of free electrons of the Au-NP as a function of wavelength of incident radiation. The energy of electron (E_0) is calculated in the range of 1.24 to 3.1 eV for the wavelength range of 400–1000 nm. Electron transmission probability with respect to Au-NP size and corresponding work function is shown in Fig. 7b. Due to increase in size of Au-NPs, the work function increases linearly in accordance with the equation: ϕ (eV) = 0.0304 $x(nm)$ + 3.3786 fitted to the data available in reference (Zhang et al. 2015). Figure 7b shows that electron transmission probability increases to small extent with increase in the NPs size till 35 nm. After 35 nm, the transmission probability decreases due to increase in barrier height. Figure 7c shows the transmission probability with respect to the wavelength of incident radiation assuming complete energy transfer from the corresponding photon to the electrons in Au-NPs. With increasing wavelength, the energy associated with the photon decreases thereby decreasing the energy of the electron in Au-NP with a decrease in corresponding transmission probability.

Amperometric current-time analysis

The amperometric (I-t) curves shown in Fig. 8a, for a configuration given in Fig. 1 are recorded at a constant potential of 0 V with the light turning ON/OFF every 30 s. The nature of photocurrent growth and decay due to illumination has been studied with fixed light intensity throughout the experiment (20 mW/cm^2). The number of photons with respect to wavelength for incident light is shown in the Fig. 8b. The current increase immediately when the light is turned on and fall back when the light is turned off. During the measurement, light is switched ON after 30th s and remains ON till 60th s, so the photocurrent starts to grow from the dark value. After attaining the highest value, the light is switched OFF at 60th s and the photocurrent instantly starts to decay and almost reaches to the initial dark value. To understand the correlation between LSPR light absorption in TiO_2-NR/Au-NP system and correspondingly generated photocurrent density, incident photon-to-current-conversion efficiency (IPCE) measurements have been performed using an equipment from Opto Solar GmbH. Clearly, the TiO_2-NR/Au-NP system exhibited obvious photocurrent enhancement as compared to the bare TiO_2-NR in the wavelength range of 400–700 nm as shown in Fig. 8c. To analyse the behaviour of
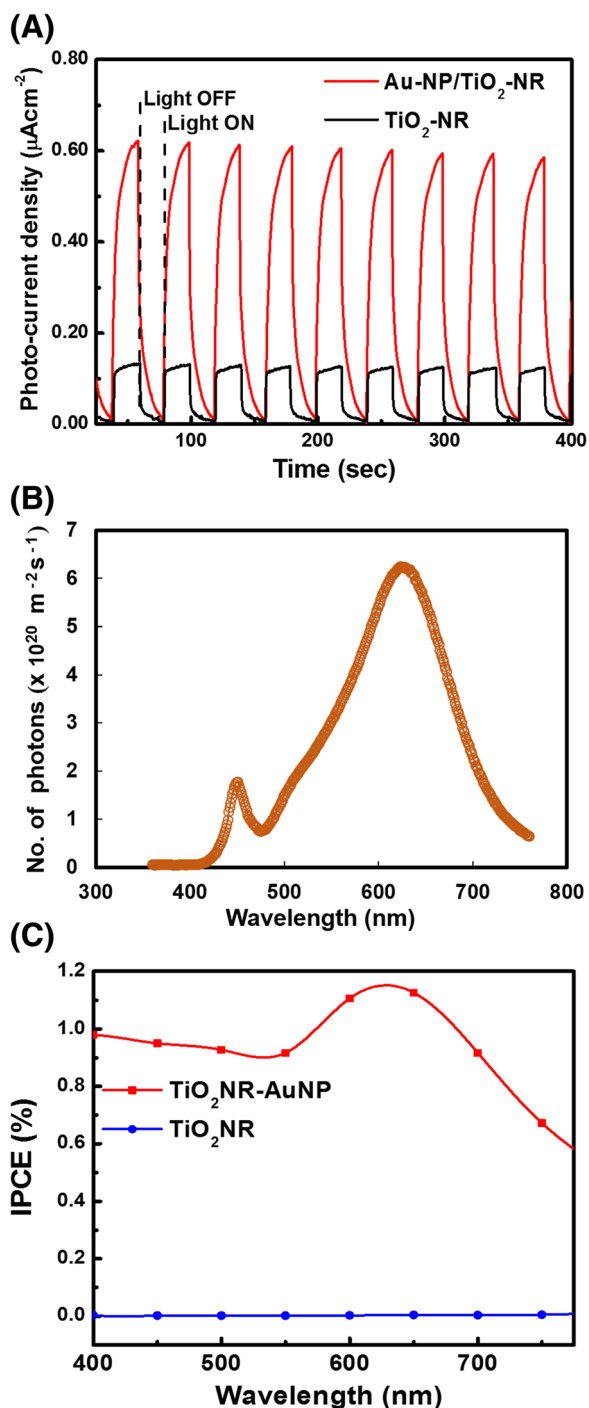
Fig. 8 **a** I-t (current-time) curves of TiO_2-NR and Au-NP/TiO_2-NR samples from amperometric measurements. **b** Number of photons with respect to the wavelength of incident light. **c** IPCE of TiO_2-NR & TiO_2-NR/Au-NP

the photocurrent, the growth and decay portion of the experimental curve has been analysed separately as shown in Fig. 9. Growth current shown in Fig. 9 clearly indicates
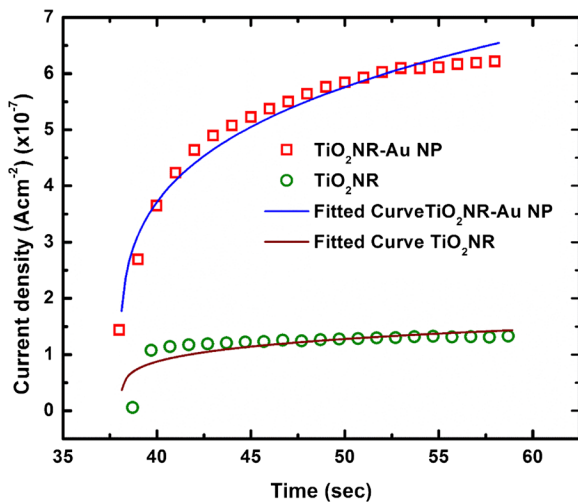
Fig. 9 Current growth analysis for TiO$_2$-NR and Au-NP/TiO$_2$-NR

the power law relation between current and time which follows following expression (Islam et al. 2012):

$$I(t) = A \times |t - t_c|^{\alpha} \qquad (9)$$

The experimental data is fitted using Eq. (9) with an acceptable range of R^2 from 0.7 to 0.9 as shown in Fig. 9. Here t_c value is 38 and t is in time (sec). The Values of α are 0.24 and 0.21, and A is 3.14×10^{-7} and 7.66×10^{-8} for the TiO$_2$-Au and TiO$_2$-NR respectively. Under visible light illumination, the catalytic activity of TiO$_2$-NRs is improved by the Au-NP plasmon-induced charge separation, which is indicated by a higher current as compared to the bare TiO$_2$ sample.

Clearly, the TiO$_2$-NR produced little photocurrent density, < 3 μAcm^{-2}, which is just above the background dark current Fig. 9. As expected, a significant photocurrent density enhancement has been observed on the Au-NP/TiO$_2$-NR, with a photocurrent density of ~ 150 μAcm^{-2} under otherwise the same conditions, which is 50 times the one with the bare TiO$_2$-NR and is much higher photocurrent density.

The much improved photocurrent density on the Au-NP/TiO$_2$-NR relative to the TiO$_2$-NR is attributed to enhanced electron density in the conduction band of TiO$_2$-NRs, which boosts the catalytic performance under visible light irradiation. The enhanced photocurrent density may be further attributed to the minimization of the thermodynamic free energy of the system, which leads to an electrostatic surface potential on a resonant

Au-NP, driven by an increase in the absorption Fig. 2 as a result of electron injection (van de Groep et al. 2016).

A high absorption does not always lead to high photo-catalytic efficiency. A more convincing proof of the plasmonic enhancement is the coincidence of the absorption peak of LSPR with the maximum wavelength region of apparent quantum efficiency according to available literature (Ohtani 2008). In a recent article, Kowalska et al. showed a clear correlation between the absorption spectrum and the quantum efficiency of Au/TiO$_2$ samples (Kowalska et al. 2009; Kowalska et al. 2010). The apparent quantum efficiency is the ratio of the number of consumed electrons to the number of incoming photons (not considering the losses of photons by reflection and transmission). For small noble metal nanoparticles (typically < 60 nm), the Mie scattering is negligible compared to the absorption (Bian et al. 2013; Hodak et al. 2000). Generally, the photons penetrate a few nanometers to a few micrometers into the semiconductor photocatalyst, and thus not all are absorbed effectively. Besides, photons absorbed far below the surface of the semiconductor contribute little to the photo-reaction since the generated electrons and holes need to have a long diffusion length and in TiO$_2$ they mostly recombine before reaching the surface. So this study demonstrated the enhancement of the absorption of visible light by Au nanoparticles and its correlation with the observed photocurrent density.

Conclusions

In this work, LSPR and electron transfer behaviour of Au-NPs attached to TiO$_2$-NRs have been studied for their optoelectronic device applications. TiO$_2$-NRs with Au-NPs exhibited a significant photocurrent enhancement as compared to the bare TiO$_2$-NRs. An increase in the photocurrent in amperometric studies has been explained on the basis of excess electron density in the CB of TiO$_2$-NR due to hot electron transfer from the attached Au-NPs. The hybrid nanostructure's deposition on the transparent substrates demonstrated in this study is suitable for versatile applications.

Compliance with ethical standards

Conflict of interest The authors declare that they have no conflict of interest.

References

Awazu K, Fujimaki M, Rockstuhl C, Tominaga J, Murakami H, Ohki Y, Yoshida N, Watanabe T (2008) A plasmonic photocatalyst consisting of silver nanoparticles embedded in titanium dioxide. J Am Chem Soc 130(5):1676–1680. https://doi.org/10.1021/ja076503n

Baker DR, Kamat PV (2009) Photosensitization of TiO_2 nanostructures with CdS quantum dots: particulate versus tubular support architectures. Adv Funct Mater 19(5):805–811. https://doi.org/10.1002/adfm.200801173

Bian Z, Tachikawa T, Zhang P, Fujitsuka M, Majima T (2013) Au/TiO_2 superstructure-based plasmonic photocatalysts exhibiting efficient charge separation and unprecedented activity. J Am Chem Soc 136:458–465

Bing Z, Dong-Sheng L, Lue-Lue X, De-Ren Y (2010) Enhanced optical absorption of amorphous silicon films by Ag nanostructures. Chin Phys Lett 27(3):037303. https://doi.org/10.1088/0256-307X/27/3/037303

Bohren CF, Huffman DR (2007) Absorption and scattering of light by small particles. Wiley-VCH, Verlag GmbH. https://doi.org/10.1002/9783527618156; http://onlinelibrary.wiley.com/book/10.1002/9783527618156

Burda C, Chen X, Narayanan R, El-Sayed MA (2005) Chemistry and properties of nanocrystals of different shapes. Chem Rev 105(4):1025–1102. https://doi.org/10.1021/cr030063a

Chen X, Mao SS (2007) Titanium dioxide nanomaterials: synthesis, properties, modifications, and applications. Chem Rev 107(7):2891–2959. https://doi.org/10.1021/cr0500535

Chen J, Cui X, Wang Q, Wang H, Zheng X, Liu C, Xue T, Wang S, Zheng W (2012) One-pot photochemical synthesis of ultrathin Au nanocrystals on co-reduced graphene oxide and its application. J Colloid Interface Sci 383(1):140–147. https://doi.org/10.1016/j.jcis.2012.06.007

Cherevko S, Kulyk N, Chung C-H (2012) Utilization of surface active sites on gold in preparation of highly reactive interfaces for alcohols electrooxidation in alkaline media. Electrochim Acta 69:190–196. https://doi.org/10.1016/j.electacta.2012.02.094

Cui C-H, Yu J-W, Li H-H, Gao M-R, Liang H-W, Yu S-H (2011) Remarkable enhancement of electrocatalytic activity by tuning the interface of Pd–Au bimetallic nanoparticle tubes. ACS Nano 5(5):4211–4218. https://doi.org/10.1021/nn2010602

Dutta A, Mahapatra SS, Datta J (2011) High performance PtPdAu nano-catalyst for ethanol oxidation in alkaline media for fuel cell applications. Int J Hydrog Energy 36(22):14898–14906. https://doi.org/10.1016/j.ijhydene.2011.02.101

El-Sayed MA (2001) Some interesting properties of metals confined in time and nanometer space of different shapes. Acc Chem Res 34(4):257–264. https://doi.org/10.1021/ar960016n

Erwin WR, Zarick HF, Talbert EM, Bardhan R (2016) Light trapping in mesoporous solar cells with plasmonic nanostructures. Energy Environ Sci 9(5):1577–1601. https://doi.org/10.1039/C5EE03847B

Evanoff DD, Chumanov G (2005) Synthesis and optical properties of silver nanoparticles and arrays. ChemPhysChem 6(7):1221–1231. https://doi.org/10.1002/cphc.200500113

Feldstein MJ, Keating CD, Liau Y-H, Natan MJ, Scherer NF (1997) Electronic relaxation dynamics in coupled metal nanoparticles. J Am Chem Soc 119(28):6638–6647. https://doi.org/10.1021/ja964098m

Feng X, Ruan F, Hong R, Ye J, Hu J, Hu G, Yang Z (2011) Synthetically directed self-assembly and enhanced surface-enhanced Raman scattering property of twinned crystalline Ag/Ag homojunction nanoparticles. Langmuir 27(6):2204–2210. https://doi.org/10.1021/la1050207

Feng D, Zhou W, Qiao X, Albert J (2016) High resolution fiber optic surface plasmon resonance sensors with single-sided gold coatings. Opt Express 24(15):16456–16464. https://doi.org/10.1364/OE.24.016456

Fu S, Zhu C, Du D, Lin Y (2015) Facile one-step synthesis of three-dimensional Pd–Ag bimetallic alloy networks and their electrocatalytic activity toward ethanol oxidation. ACS Appl Mater Interfaces 7(25):13842–13848. https://doi.org/10.1021/acsami.5b01963

Ghatak A (2010) Basic quantum mechanics. Macmillan Publishers India Limited, New Delhi

Hodak JH, Henglein A, Hartland GV (2000) Photophysics of nanometer sized metal particles: electron-phonon coupling and coherent excitation of breathing vibrational modes. J Phys Chem B 104(43):9954–9965. https://doi.org/10.1021/jp002256x

Huang X, El-Sayed MA (2010) Gold nanoparticles: optical properties and implementations in cancer diagnosis and photothermal therapy. J Adv Res 1(1):13–28. https://doi.org/10.1016/j.jare.2010.02.002

Huang HJ, Zhen S-Y, Li P-Y, Tzeng S-D, Chiang H-P (2016) Confined migration of induced hot electrons in Ag/graphene/TiO_2 composite nanorods for plasmonic photocatalytic reaction. Opt Express 24(14):15603–15608. https://doi.org/10.1364/OE.24.015603

Hutter E, Fendler JH (2004) Exploitation of localized surface plasmon resonance. Adv Mater 16(19):1685–1706. https://doi.org/10.1002/adma.200400271

Ingram DB, Linic S (2011) Water splitting on composite plasmonic-metal/semiconductor photoelectrodes: evidence for selective plasmon-induced formation of charge carriers near the semiconductor surface. J Am Chem Soc 133(14):5202–5205. https://doi.org/10.1021/ja200086g

Islam MR, Maity S, Haldar A, Manik N, Basu A (2012) Photocurrent growth and decay behavior of crystal violet dye-based photoelectrochemical cell in photovoltaic mode. Ionics 18(1-2):209–214. https://doi.org/10.1007/s11581-011-0586-7

Jain PK, Lee KS, El-Sayed IH, El-Sayed MA (2006) Calculated absorption and scattering properties of gold nanoparticles of different size, shape, and composition: applications in biological imaging and biomedicine. J Phys Chem B 110(14):7238–7248. https://doi.org/10.1021/jp057170o

Jin Z, Wang Q, Zheng W, Cui X (2016) Highly ordered periodic Au/TiO_2 hetero-nanostructures for plasmon-induced enhancement of the activity and stability for ethanol electro-

oxidation. ACS Appl Mater Interfaces 8(8):5273–5279. https://doi.org/10.1021/acsami.5b11259

Kim H-S, Lee JW, Yantara N, Boix PP, Kulkarni SA, Mhaisalkar S, Grätzel M, Park NG (2013a) High efficiency solid-state sensitized solar cell-based on submicrometer rutile TiO$_2$ nanorod and CH3NH3PbI3 perovskite sensitizer. Nano Lett 13(6):2412–2417. https://doi.org/10.1021/nl400286w

Kim K, Thiyagarajan P, Ahn H-J, Kim S-I, Jang J-H (2013b) Optimization for visible light photocatalytic water splitting: gold-coated and surface-textured TiO 2 inverse opal nano-networks. Nano 5:6254–6260

Kowalska E, Abe R, Ohtani B (2009) Visible light-induced photocatalytic reaction of gold-modified titanium(iv) oxide particles: action spectrum analysis. Chem Commun 0:241–243. https://doi.org/10.1039/B815679D

Kowalska E, Mahaney OOP, Abe R, Ohtani B (2010) Visible-light-induced photocatalysis through surface plasmon excitation of gold on titania surfaces. Phys Chem Chem Phys 12(10):2344–2355. https://doi.org/10.1039/b917399d

Lee C-H, Liao SC, Lin TR, Wang SH, Lai DY, Chiu PK, Lee JW, Wu WF (2016) Boosted photocatalytic efficiency through plasmonic field confinement with bowtie and diabolo nano-structures under LED irradiation. Opt Express 24(16): 17541–17552. https://doi.org/10.1364/OE.24.017541

Liang ZX, Zhao TS, Xu JB, Zhu LD (2009) Mechanism study of the ethanol oxidation reaction on palladium in alkaline media. Electrochim Acta 54(8):2203–2208. https://doi.org/10.1016/j.electacta.2008.10.034

Liang YQ, Cui ZD, Zhu SL, Liu Y, Yang XJ (2011) Silver nanoparticles supported on TiO$_2$ nanotubes as active catalysts for ethanol oxidation. J Catal 278(2):276–287. https://doi.org/10.1016/j.jcat.2010.12.011

Lidia A et al (2007) Photocatalytic and antibacterial activity of TiO$_2$ and Au/TiO$_2$ nanosystems. Nanotechnology 18:375709

Lin S, Li M, Dujardin E, Girard C, Mann S (2005) One-dimensional plasmon coupling by facile self-assembly of gold nanoparticles into branched chain networks. Adv Mater 17(21):2553–2559. https://doi.org/10.1002/adma.200500828

Linic S, Christopher P, Ingram DB (2011) Plasmonic-metal nano-structures for efficient conversion of solar to chemical energy. Nat Mater 10(12):911–921. https://doi.org/10.1038/nmat3151

Liu G, Wang L, Yang HG, Cheng H-M, Lu GQ (2010) Titania-based photocatalysts-crystal growth, doping and heterostructuring. J Mater Chem 20(5):831–843. https://doi.org/10.1039/B909930A

Liu Z, Hou W, Pavaskar P, Aykol M, Cronin SB (2011) Plasmon resonant enhancement of photocatalytic water splitting under visible illumination. Nano Lett 11(3):1111–1116. https://doi.org/10.1021/nl104005n

Long PD, Chien DT, Trung NT, Hieu NS, Chi LH, Van Cat V, Lam VD (2017) Plasmonic effect enhanced photocurrent in nano-structured TiO2 films decorated with gold nanoparticles. J Electron Mater 46(7):4448–4454. https://doi.org/10.1007/s11664-017-5436-6

Murdoch M, Waterhouse GIN, Nadeem MA, Metson JB, Keane MA, Howe RF, Llorca J, Idriss H (2011) The effect of gold loading and particle size on photocatalytic hydrogen production from ethanol over Au/TiO$_2$ nanoparticles. Nat Chem 3(6):489–492. https://doi.org/10.1038/nchem.1048

Nayak J, Prabakar K, Park J, Kim H (2012) Effect of synthesis temperature on structure, optical and photovoltaic properties of TiO$_2$ nanorod thin films. Electrochim Acta 65:44–49. https://doi.org/10.1016/j.electacta.2012.01.012

Ohtani B (2008) Preparing articles on photocatalysis-beyond the illusions, misconceptions, and speculation. Chem Lett 37(3): 216–229. https://doi.org/10.1246/cl.2008.216

Oliveira MC, Rego R, Fernandes LS, Tavares PB (2011) Evaluation of the catalytic activity of Pd–Ag alloys on ethanol oxidation and oxygen reduction reactions in alkaline medium. J Power Sources 196(15):6092–6098. https://doi.org/10.1016/j.jpowsour.2011.03.062

Paramasivam I, Macak JM, Schmuki P (2008) Photocatalytic activity of TiO$_2$ nanotube layers loaded with Ag and Au nanoparticles electrochemistry. Communications 10(1):71–75. https://doi.org/10.1016/j.elecom.2007.11.001

Park N-G, Schlichthörl G, Van de Lagemaat J, Cheong H, Mascarenhas A, Frank A (1999) Dye-sensitized TiO$_2$ solar cells: structural and photoelectrochemical characterization of nanocrystalline electrodes formed from the hydrolysis of TiCl4. J Phys Chem B 103(17):3308–3314. https://doi.org/10.1021/jp984529i

Qi K, Wang Q, Zheng W, Zhang W, Cui X (2014) Porous single-crystalline palladium nanoflowers with enriched {100} facets for highly enhanced ethanol oxidation. Nano 6(24):15090–15097. https://doi.org/10.1039/C4NR05761A

Raval D, Tripathi B, Ray A (2016) Titanium dioxide nanorod diameter and layer porosity optimization by estimating electrical performance of dye and perovskite sensitized solar cell. J Porous Mater 24(1):1–15. https://doi.org/10.1007/s10934-016-0255-3

Reineck P, Brick D, Mulvaney P, Bach U (2016) Plasmonic hot electron solar cells: the effect of nanoparticle size on quantum efficiency. J Phys Chem Lett 7(20):4137–4141. https://doi.org/10.1021/acs.jpclett.6b01884

Rifat AA, Mahdiraji GA, Sua YM, Ahmed R, Shee YG, FRM A (2016) Highly sensitive multi-core flat fiber surface plasmon resonance refractive index sensor. Opt Express 24(3):2485–2495. https://doi.org/10.1364/OE.24.002485

Rycenga M, Cobley CM, Zeng J, Li W, Moran CH, Zhang Q, Qin D, Xia Y (2011) Controlling the synthesis and assembly of silver nanostructures for plasmonic applications. Chem Rev 111(6):3669–3712. https://doi.org/10.1021/cr100275d

Sarkar D, Ghosh CK, Chattopadhyay KK (2012) Morphology control of rutile TiO$_2$ hierarchical architectures and their excellent field emission properties. CrystEngComm 14(8): 2683–2690. https://doi.org/10.1039/C2CE06392A

Sciancalepore C, Cassano T, Curri ML, Mecerreyes D, Valentini A, Agostiano A, Tommasi R, Striccoli M (2008) TiO$_2$ nanorods/PMMA copolymer-based nanocomposites: highly homogeneous linear and nonlinear optical material. Nanotechnology 19(20):205705. https://doi.org/10.1088/0957-4484/19/20/205705

Sun X, Dai D, Thylén L, Wosinski L (2015) High-sensitivity liquid refractive-index sensor based on a Mach-Zehnder interferometer with a double-slot hybrid plasmonic waveguide. Opt Express 23(20):25688–25699. https://doi.org/10.1364/OE.23.025688

Tada H, Mitsui T, Kiyonaga T, Akita T, Tanaka K (2006) All-solid-state Z-scheme in CdS-Au-TiO$_2$ three-component nanojunction system. Nat Mater 5(10):782–786 http://www.

nature.com/nmat/journal/v5/n10/suppinfo/nmat1734_S1. html. https://doi.org/10.1038/nmat1734

Thimsen E, Le Formal F, Grätzel M, Warren SC (2011) Influence of plasmonic Au nanoparticles on the photoactivity of Fe2O3 electrodes for water splitting. Nano Lett 11(1):35–43. https://doi.org/10.1021/nl1022354

Tian Y, Tatsuma T (2005) Mechanisms and applications of plasmon-induced charge separation at TiO$_2$ films loaded with gold nanoparticles. J Am Chem Soc 127(20):7632–7637. https://doi.org/10.1021/ja042192u

Tripathi B, Yadav P, Kumar M (2013) Plasmon-enhanced light trapping to improve efficiency of TiO$_2$ nanorod-based dye-sensitized solar cell. Plasmonics 8(3):1501–1507. https://doi.org/10.1007/s11468-013-9564-4

van de Groep J, Sheldon MT, Atwater HA, Polman A (2016) Thermodynamic theory of the plasmoelectric effect. Sci Rep 6:23283. https://doi.org/10.1038/srep23283

Wang H, Bai Y, Zhang H, Zhang Z, Li J, Guo L (2010) CdS quantum dots-sensitized TiO$_2$ nanorod array on transparent conductive glass photoelectrodes. J Phys Chem C 114(39): 16451–16455. https://doi.org/10.1021/jp104208z

Wang H, You T, Shi W, Li J, Guo L (2012) Au/TiO$_2$/Au as a plasmonic coupling photocatalyst. J Phys Chem C 116(10): 6490–6494. https://doi.org/10.1021/jp212303q

Wang Q, Cui X, Guan W, Zhang X, Liu C, Xue T, Wang H, Zheng W (2014) A nanoflower shaped gold-palladium alloy on graphene oxide nanosheets with exceptional activity for electrochemical oxidation of ethanol. Microchim Acta 181(3-4): 373–380. https://doi.org/10.1007/s00604-013-1119-z

Warren SC, Thimsen E (2012) Plasmonic solar water splitting. Energy Environ Sci 5(1):5133–5146. https://doi.org/10.1039/C1EE02875H

Westcott S, Jackson J, Radloff C, Halas N (2002) Relative contributions to the plasmon line shape of metal nanoshells. Phys Rev B 66(15):155431. https://doi.org/10.1103/PhysRevB.66.155431

Wu J-L, Chen FC, Hsiao YS, Chien FC, Chen P, Kuo CH, Huang MH, Hsu CS (2011) Surface plasmonic effects of metallic nanoparticles on the performance of polymer bulk heterojunction solar cells. ACS Nano 5(2):959–967. https://doi.org/10.1021/nn102295p

Xu C, Pk S, Liu Y (2007a) Ethanol electrooxidation on Pt/C and Pd/C catalysts promoted with oxide. J Power Sources 164(2): 527–531. https://doi.org/10.1016/j.jpowsour.2006.10.071

Xu CW, Wang H, Shen PK, Jiang SP (2007b) Highly ordered Pd nanowire arrays as effective electrocatalysts for ethanol oxidation in direct alcohol fuel cells. Adv Mater 19(23):4256–4259. https://doi.org/10.1002/adma.200602911

Xu Z, Li C, Kang X, Yang D, Yang P, Hou Z, Lin J (2010) Synthesis of a multifunctional nanocomposite with magnetic, mesoporous, and near-IR absorption properties. J Phys Chem C 114(39):16343–16350. https://doi.org/10.1021/jp106325c

Xu Z, Yu J, Liu G (2011) Enhancement of ethanol electrooxidation on plasmonic Au/TiO 2 nanotube arrays. Electrochem Commun 13(11):1260–1263. https://doi.org/10.1016/j.elecom.2011.08.029

Yen YC, Chen JA, Ou S, Chen YS, Lin KJ (2017) Plasmon-enhanced photocurrent using gold nanoparticles on a three-dimensional TiO2 nanowire-web electrode. Sci Rep 7:42524. https://doi.org/10.1038/srep42524

Zhang F, Liu X (1998) Effect of O 2 pressure on the preferred orientation of TiO$_2$ films prepared by filtered arc deposition. Thin Solid Films 326(1-2):171–174. https://doi.org/10.1016/S0040-6090(98)00573-2

Zhang H, Wang G, Chen D, Lv X, Li J (2008) Tuning photoelectrochemical performances of Ag−TiO$_2$ nanocomposites via reduction/oxidation of Ag. Chem Mater 20(20): 6543–6549. https://doi.org/10.1021/cm801796q

Zhang Z, Zhang L, Hedhili MN, Zhang H, Wang P (2012) Plasmonic gold nanocrystals coupled with photonic crystal seamlessly on TiO$_2$ nanotube photoelectrodes for efficient visible light photoelectrochemical water splitting. Nano Lett 13:14–20

Zhang Y, Pluchery O, Caillard L, Lamic-Humblot A-F, Casale S, Chabal YJ, Salmeron M (2015) Sensing the charge state of single gold nanoparticles via work function measurements. Nano Lett 15(1):51–55. https://doi.org/10.1021/nl503782s

Zhang M, Hu DJJ, Shum PP, Wu Z, Li K, Huang T, Wei L (2016) High-birefringent microstructured optical fiber based surface plasmon resonance sensor. In: Conference on Lasers and Electro-Optics, San Jose, California, 2016/06/05 2016. OSA Technical Digest (online). Opt Soc Am JTu5A.116. https://doi.org/10.1364/CLEO_AT.2016.JTu5A.116

Zhao L, Thomas JP, Heinig NF, Abd-Ellah M, Wang X, Leung KT (2014) Au–Pt alloy nanocatalysts for electro-oxidation of methanol and their application for fast-response non-enzymatic alcohol sensing. J Mater Chem C 2(15):2707. https://doi.org/10.1039/c3tc32317j

Zhou W, Zhou Z, Song S, Li W, Sun G, Tsiakaras P, Xin Q (2003) Pt based anode catalysts for direct ethanol fuel cells. Appl Catal B Environ 46(2):273–285. https://doi.org/10.1016/S0926-3373(03)00218-2

Zhu C, Guo S, Dong S (2012) PdM (M= Pt, Au) bimetallic alloy nanowires with enhanced electrocatalytic activity for electro-oxidation of small molecules. Adv Mater 24(17):2326–2331. https://doi.org/10.1002/adma.201104951